J Nanostruct 14(3): 857-874, Summer 2024

RESEARCH PAPER

Preparation of Nano Lignin–Based Activated Carbon Depending on Ratio Impregnation of K_2CO_3, Activation Time and Activation Temperature on Yield for Congo Red Dye Adsorption

Masar Mohammed Abd Alhussein and Nahla Shakir Salman *

Department of Chemistry, College of Education, University of Al-Qadisiyah, Diwaniyah, Iraq

ARTICLE INFO

Article History:
Received 05 April 2024
Accepted 24 June 2024
Published 01 July 2024

Keywords:
Activated carbon
Adsorption
Congo red (CR) dye
K_2CO_3
Lignin

ABSTRACT

This study involves the synthesis of nano form of activated carbon (AC) adsorbent derived from agricultural biomass (lignin) for effective removal of congo red (CR) dye from water. Chemical activation using potassium carbonate (K_2CO_3) was employed for transforming lignin into AC. The effects of impregnation ratio, activation time, and temperature on adsorbent's properties were studied. Characterization techniques, including FTIR, XRD, SEM-EDX, BET-BJH, and TEM, highlighted the successful synthesis of activated carbon with a porous structure. Results revealed that the optimal AC, prepared with a K_2CO_3/lignin ratio of 2:1, demonstrated excellent adsorption capabilities for CR dye removal. Various parameters including contact time, adsorbent dose, pH, and temperature were evaluated to determine the optimal conditions for maximum dye removal efficiency. The results indicated a maximum removal efficiency of 89.93% under optimized conditions. Thermodynamic study revealed the endothermic and spontaneous nature of studied process. Isotherm models such as Langmuir, Freundlich, and Temkin models revealed that the Langmuir model best described the adsorption behaviour, suggesting a chemisorption mechanism. Additionally, the kinetic studies further supported the pseudo-second-order model, highlighting the chemical-controlled adsorption process. Overall, results showed the promising nature of synthesized adsorbent for CR dye removal.

How to cite this article
Abd Alhussein M., Salman N. Preparation of Nano Lignin–Based Activated Carbon Depending on Ratio Impregnation of K_2CO_3, Activation Time and Activation Temperature on Yield for Congo Red Dye Adsorption . J Nanostruct, 2024; 14(3):857-874.
DOI: 10.22052/JNS.2024.03.016

INTRODUCTION

Water pollution is one of the serious environmental problems that threaten both human health and economic development [1]. Dyeing, pulp and paper, plastic, cosmetic, leather and food industries make use of dyes for staining products. The photolytic and chemical stability of dyes make them resistant towards degradation that ultimately led to water pollution [2, 3]. Increased human and industrial activities have led to various types of pollutants, such as organic, inorganic dyes and heavy metal ions [4]. Numerous technologies have been employed for mitigating water pollution, such as ozonation, sonocatalysis, photocatalysis, membrane filtration, ion exchange, electrochemical processes, and adsorption [5-16]. Among these techniques, adsorption has gained popularity due to its low cost, biodegradability,

* *Corresponding Author Email: nahla.shaker@qu.edu.iq*

and eco-friendliness [17-19]. Important performance indicators for adsorption systems include adsorption capacity and adsorption rate. Different types of adsorbent materials have been investigated for the effective removal of dyes such as congo red (CR) dye [20]. Congo Red (CR) is a synthetic anionic azo dye derived mainly from benzidine. Continuous exposure to CR can lead to allergic reactions and its metabolism can produce benzidine, a known carcinogen. Its molecular structure in water can vary depending on pH that thereby affects its removal efficiency [21-23].

Activated carbon (AC) has proven to be a highly effective and widely used adsorbent for treating dye wastewater and removing various pollutants dissolved in water. Derived from agricultural waste and natural materials including rice husk, coconut shell, bituminous coal, and lignite, AC shows exceptional surface area and total pore volume, making it well-suited for adsorption applications [24, 25]. Lignin, a polyphenolic agro-waste having an amorphous structure and high surface area, is a promising precursor for the development of high-value products. Its complex structure, characterized by the presence of different ionic functional groups (including hydroxyl, phenolic, and carboxyl), makes it a versatile starting material. Lignin-derived activated materials have gained significant attention in recent years. The preparation of AC from lignin involves thermal processes including carbonization and activation. Activation process can be achieved through either physical or chemical ways. During carbonization, the temperature is increased to high levels i.e., 400-900 °C while chemical activation often involves the use of various agents such as H_3PO_4, $ZnCl_2$, KOH, K_2CO_3 [26-28].

Keeping in view the above discussion, this study focuses on the synthesis of nano form of activated carbon from lignin, a natural source obtained from straw pulping, using both physical and chemical activation methods. Chemical activation was performed using potassium carbonate (K_2CO_3). The optimal synthesis parameters, such as mass ratio of potassium compound to lignin, activation temperature, and time, were investigated. Characterization of the activated carbon synthesized under optimal conditions with K_2CO_3 was conducted using Fourier transform-infrared spectroscopy (FT-IR), X-ray diffraction (XRD), transmission electron microscopy (TEM), Field emission scanning electron microscopy (FESEM), Brunauer-Emmett-Teller/ Barrett-Joyner-Halenda (BET/ BJH) analysis, and energy-dispersive X-ray spectroscopy (EDX). The adsorption behaviour of the synthesized activated carbon towards CR dye removal from water was also investigated. The effects of contact time, adsorbent dosage, initial pH, and temperature were studied, along with kinetic and thermodynamic studies to assess the dye adsorption efficiency.

MATERIALS AND METHODS

Materials

Lignin, a precursor obtained from straw pulping, was sourced from a local farm (shown in Fig. 1). Analytical-grade potassium carbonate (K_2CO_3) and CR dye were procured from Scharlau. Double-distilled water was used to prepare aqueous solutions for the experiments.

Preparation of activated carbon (AC)

Preparation of raw materials

Lignin, a precursor obtained from straw pulping,

Fig. 1. Straw pulping used in experiment.

was collected from a local farm in Al-Diwaniyah city, southern Iraq. The samples were washed thoroughly with double-distilled water (DDW) to remove any kind of impurities present and then oven-dried at 105°C for 4 hours.

Preparation of nano AC based lignin

Activated carbon was produced from lignin using a combination of both physical and chemical activation methods. Physical activation method involved pyrolysis to obtain char, followed by chemical activation with potassium carbonate (K_2CO_3). An accurately weighed 2 g of oven-dried lignin powder was impregnated with various mass ratios of K_2CO_3 (including 0.5:1, 1:1, 1.5:1, 2:1, and 2.5:1) in 20% aqueous solutions and placed in a crucible for the time period of 16 hours. The mixtures were then dried and dehydrated in an electric furnace. Carbonization process of the impregnated samples was conducted at temperatures varying from 450°C to 850°C for 20-60 minutes under a nitrogen atmosphere, with the heating rate of 200°C/ min. After activation with K_2CO_3, the chemical activating agent was removed by washing the samples multiple times with hot and cold distilled water until the washing water reached a neutral pH as measured by the pH meter. The liquid phase was then removed by centrifugation at 6000 rpm. Finally, the activated carbon nanoparticles were dried in an oven at 105 °C for the time period of 6 hours [29, 30]. The yield of activated carbon was calculated using the following equation [3, 31]:

$$\text{Yield} = (\frac{M_1}{M_2}) \times 100\% \quad (1)$$

here, and refers to the mass of AC and the initial mass of oven-dried lignin.

Characterization

The prepared adsorbent was characterized in terms of yield and many other properties. The surface morphologies of lignin and AC were analyzed with the help of scanning electron microscopy (SEM) (Zeiss Libra 200 FE, Germany). The crystalline structures of lignin and activated carbon were studied by using X-ray diffractometry (XRD-6000, Shimadzu-Japan, 2θ range of 10° to 80°, λ=1.5405 Å). Transmission electron microscopy (TEM) images were recorded with Philips model FEL, Quanta 400. Additionally, Fourier transform infrared spectroscopy (FTIR) using a Shimadzu-8400S spectrophotometer was employed for characterization of different functional groups present in prepared adsorbent (32). The Brunauer-Emmett-Teller (BET) method was used to calculate the specific surface area based on nitrogen adsorption isotherms at variable relative pressures (P/P_0). Furthermore, pore size distribution was determined using Barrett-Joyner-Halenda (BJH) method. Elemental composition and chemical analysis were identified using energy-dispersive X-ray spectroscopy (EDX) [31, 33, 34].

Adsorption studies

The adsorption efficiency of prepared adsorbent was evaluated under various

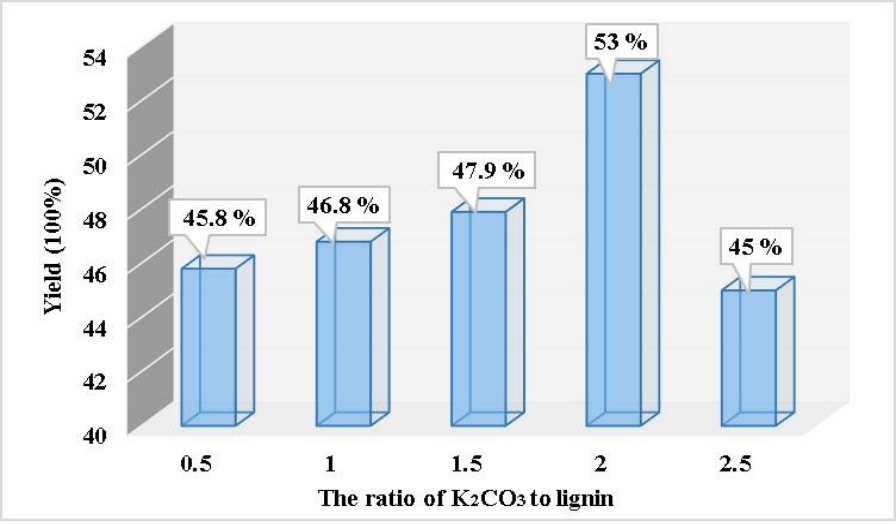

Fig. 2. Effect of K_2CO_3 ratios to lignin on yield of activated carbon.

experimental conditions, including contact time (0-45 min), adsorbent mass (0.001-0.01 g/ 25 ml), pH (4-10), initial dye concentration (50 mg/l for CR), and temperature (293-308 K). Batch adsorption experiments were conducted in conical flasks, where a known mass of activated carbon was added to 25 ml of CR dye solution. The pH of solutions was adjusted using 1 M HCl or 1 M NaOH. The mixtures were then stirred in an orbital shaker at the speed of 110 rpm for a specified time, followed by centrifugation at 6000 rpm for 10 minutes that helps in removing the adsorbent particles. The absorbance of the solutions was then measured using a UV-Visible spectrophotometer (PC 1650, Shimadzu, Japan) at the maximum wavelength (λ_{max}) of 498 nm for CR dye. This general procedure was repeated with different experimental parameters to determine the removal efficiency (% removal) and adsorption capacity (Q_e) of AC using Eqs. 2 and 3 respectively [35, 36].

$$\% \text{ removal} = \frac{(C_i - C_e)x100}{C_i} \quad (2)$$

$$Q_e = \frac{(C_i - C_e)V}{m} \quad (3)$$

where, C_i and C_e represent the initial and final concentrations of CR dye (mg/ l) respectively, V is the volume (L) of dye solution and m is the weight

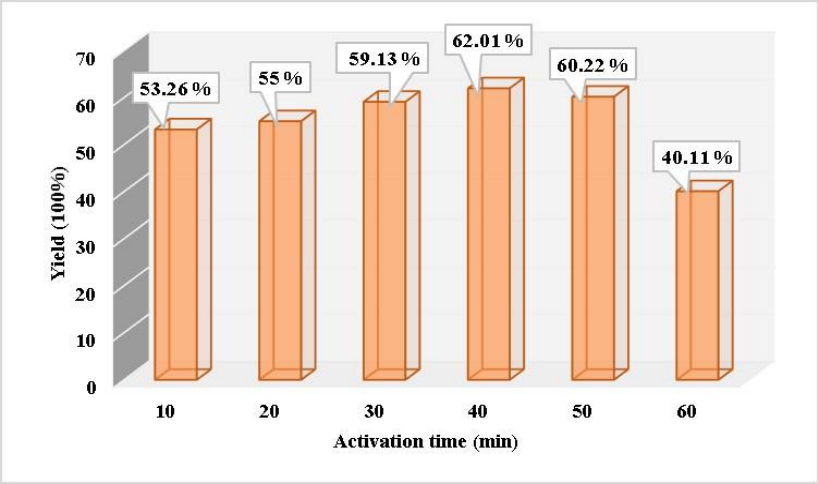

Fig. 3. Effect of activation time on yield.

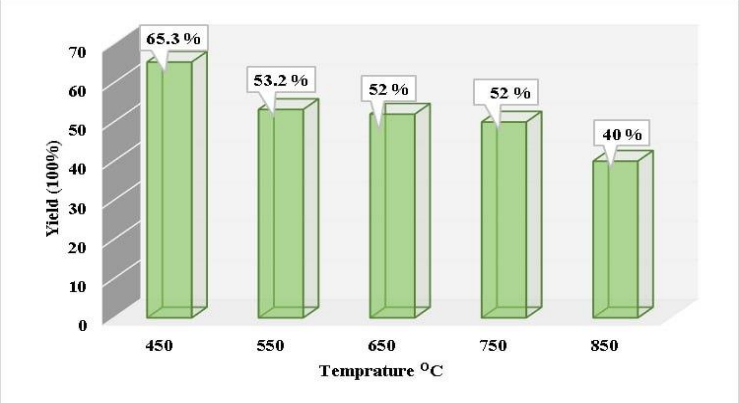

Fig. 4. Effect of activation temperature on yield.

(g) of adsorbent.

RESULTS AND DISCUSSION

Effect of activating agent ratio to lignin on yield

Product yield is a crucial metric for evaluating the impact of K_2CO_3/ lignin mass ratio on AC synthesis. AC was prepared from lignin derived from straw pulping, and the optimal conditions were determined based on adsorption properties and yield. The effects of varying the K_2CO_3/ lignin ratio between 0.5 and 2.5 were studied, resulting in yields varying from 45.8% to 45%. As highlighted in Fig. 2, increasing the K_2CO_3/ lignin ratio (with a constant lignin mass) led to a corresponding increase in yield up to a ratio of 2:1. This ratio resulted in an increase in highest product yield of 53%, demonstrating superior effectiveness and removal efficiencies. The higher yield is attributed to the formation of more pores, which increases adsorption capacity. However, adding excess K_2CO_3 at a ratio of 2.5 resulted in a decrease in yield due to additional reactions between K_2CO_3 and microporous carbon. This leading to the destruction of formed structure and increased carbon consumption [37].

Effect of activation time on yield

The effect of activation time on the yield of activated carbon (with a K_2CO_3/ lignin ratio of 2:1) was investigated under experimental conditions. As revealed in Fig. 3, the yield of activated carbon increased with increasing activation time within the range of 10 to 50 minutes, reaching a maximum of 62.22%. However, after 50 minutes, further increases in activation time resulted in wider pores and carbon burn-off thereby leading to a decrease in both yield (40.11%) and adsorption capacity.

Effect of activated temperature on yield

The K_2CO_3/ lignin ratio (2:1) and activation time (50 min) were maintained constant for evaluating the yield of AC at different temperatures ranging from 450 to 850 °C. Fig. 4 illustrates that increasing the activation temperature from 450 to 850 °C resulted in a significant decrease in carbon yield, from 65.3 % to 40 %. Within the temperature range of 450 to 750 °C, the yield decreased from 65.3 % to 52 %, accompanied by the formation of more pores [38]. However, further increases in temperature from 750 to 850 °C led to a decline in yield to 40 % due to pore widening and burn-off. The optimal temperature for synthesizing AC with a high number of pores was found to be 750 °C using K_2CO_3 as the activating agent. This activation process enhanced the adsorption capacity of AC. At higher temperatures of 850 °C, pore widening

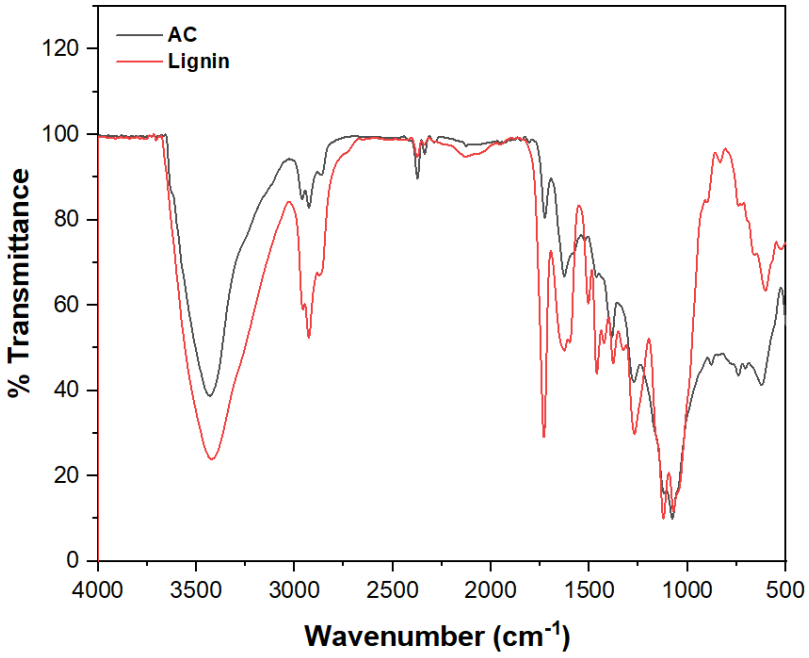

Fig. 5. FT-IR spectra of lignin and AC.

and burn-off occurred, leading to the formation of a white material (ash) and a decrease in adsorption ability [29].

Activation mechanism with chemical agent (K_2CO_3)

After alkaline pre-treatment of lignin with K_2CO_3, the sample was carbonized and activated. During activation with K_2CO_3, carbon is consumed, producing potassium metal (K) and carbon monoxide (CO). After carbonization process at 450-750 °C, gasification occurs via following reaction involving the alkali metal [39]:

$$K_2CO_3 + 2C \rightarrow 2K + 3CO \quad (4)$$

The carbon is removed as CO due to the reduction of K_2CO_3 by carbon, resulting in the products as elaborated in equation above. The surface area and pore volume increase at the optimal temperature of 750 °C. Elemental potassium decreases the shrinkage of raw material by occupying a significant volume when temperature increases. Washing with hot distilled water results in removing potassium, leaving behind micropores [40].

Characterization of activated carbon as adsorbent

FT-IR analysis

Fourier-transform infrared spectroscopy (FTIR) was used to analyze the surface functional groups of raw straw pulping and prepared AC. FTIR spectra were obtained in the mid-infrared range between 500 and 4000 cm^{-1}. Fig. 5 shows a prominent peak at 3410 cm^{-1}, indicating the stretching vibration of hydroxyl, phenolic, and carboxylic groups in lignin. A sharp peak at 2854 cm^{-1} is attributed to symmetric stretching of CH_3 group in the methoxyl group. Furthermore, a distinct peak at 1714 cm^{-1} corresponds to carbonyl stretching, associated with unconjugated carboxyl and ketone groups. The band obtained at 1033 cm^{-1} corresponds to the C-O stretching vibrations in C-OH for primary alcohols and aromatic CH [5, 41-48].

X-ray diffraction

X-ray diffraction (XRD) analysis was performed using monochromatic nickel-filtered CuKα radiation (λ = 1·5416 Å) for investigating the crystallinity of lignin and activated carbon· Fig. 6 shows the XRD patterns of raw lignin and carbon precursors impregnated with K_2CO_3. Results revealed more intense peaks in lignin when compared with AC. In activated carbon, the main peak is less intense due to presence of $KHCO_3$ and weak peaks of $K_4H_2(CO_3)_3$. This suggests the formation of C-O-K complexes, which participate in the activation reaction. The absence of sharp peaks and appearance of a broad diffraction

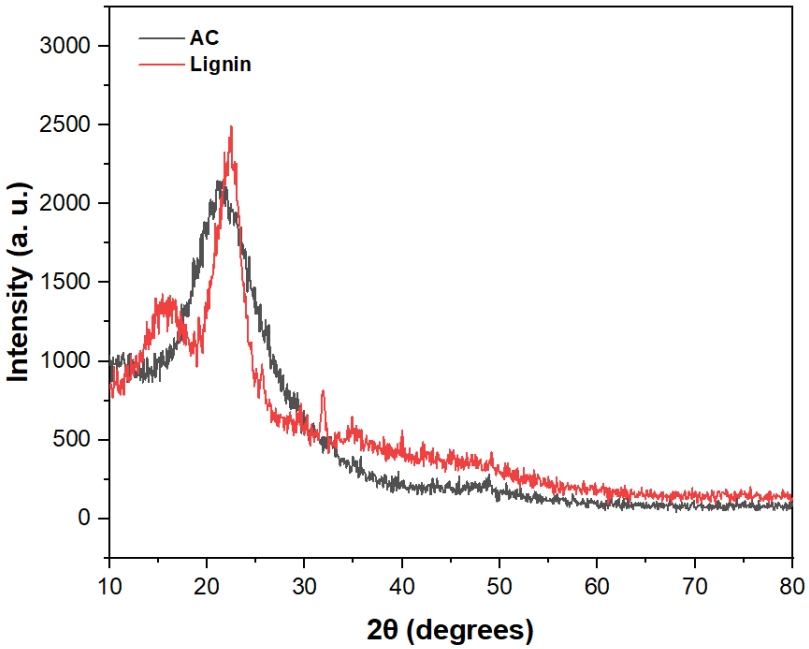

Fig. 6. XRD graph of lignin and AC.

peak in AC with K_2CO_3 indicate the presence of an amorphous structure in studied material [49, 50].

SEM-EDX analysis

The surface texture of lignin and activated carbon was examined using SEM (Fig. 7). Results revealed that the lignin exhibited a heterogeneous structure with no visible pores. Activated carbon prepared at 750 °C displayed a porous honeycomb structure exhibiting irregular shapes and sizes. The activation process, involving the formation and widening of small pores due to vaporized moisture and precursor contents, resulted in introducing the porosity in its structure [51]. Additionally, K_2CO_3 related contaminants occupied the formed cavities during pyrolysis process [52-54]. Furthermore, EDX analysis revealed the elemental composition of AC and lignin. Activated carbon contained a high percentage of carbon (50.65%), followed by oxygen (45.10%), nitrogen (3.99%), and potassium (0.26%). Lignin contained a higher carbon content (74.37%) compared to oxygen (19.66%) and nitrogen (5.98%). These results revealed that carbon is the dominant element on surface of AC [55-57].

TEM analysis

TEM images were used to analyze the surface morphology and size properties of lignin and AC (results are elaborated in Fig. 8). Study revealed that the lignin appeared as microfibrils, while AC showed the intercalation of K species within the carbon matrix. This intercalation is mainly attributed to quasi-chemical bonds, such as –O-K bond [58, 59].

BET-BJH analysis

The surface area of a solid is defined as the sum of its external surface and accessible internal pore surface. In this study, BET surface area and micropore volume were determined using N_2 adsorption experiments. The adsorption capacity

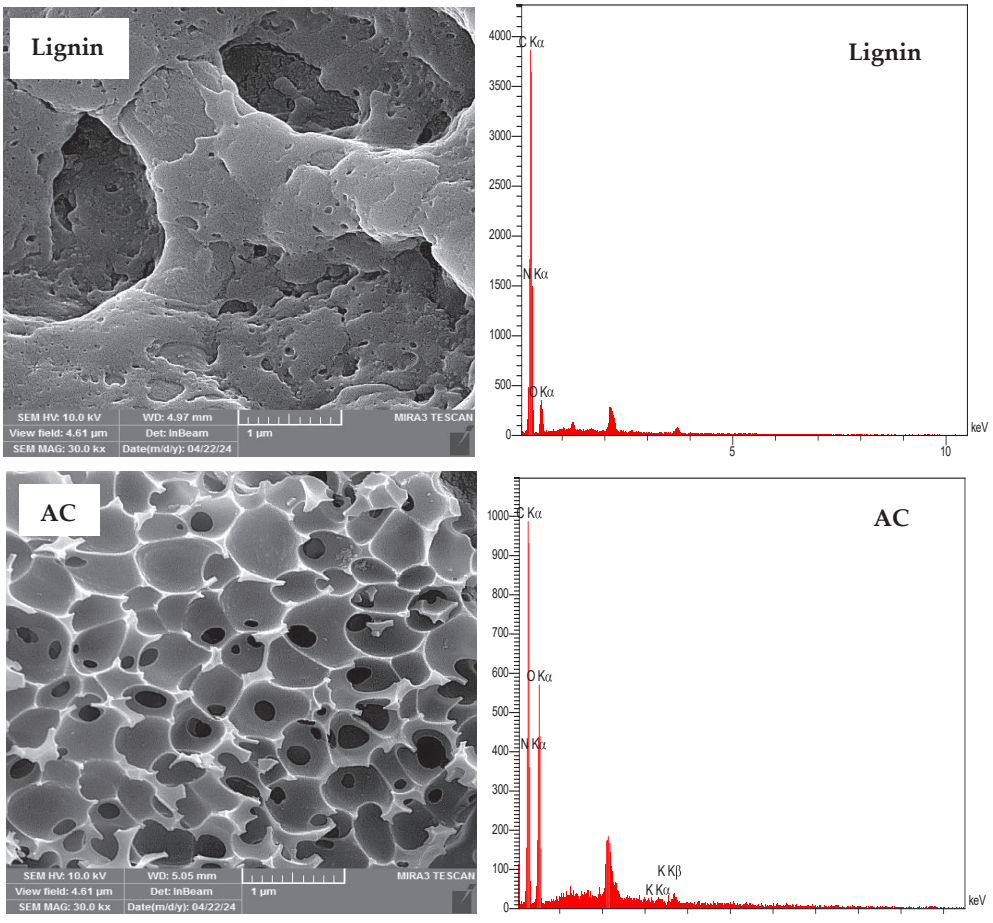

Fig. 7. SEM–EDX of lignin and AC.

of AC is directly proportional to its surface area. Fig. 9 illustrates the N_2 adsorption-desorption isotherms and pore size distribution curves for lignin and AC. Table 1 summarizes the BET surface area and pore size values. Results revealed that BET surface area increased significantly from 31.632 m²/ g for lignin to 270.42 m²/ g for AC prepared at 750 °C. Similarly, the pore volume increased from 22.125 cm³/ g to 48.841 cm³/ g. The porosity of lignin-based AC produced by chemical activation with K_2CO_3 increased with higher impregnation ratios and activation temperatures. The resulting AC exhibited a higher micropore volume. Additionally, increasing the impregnation ratio

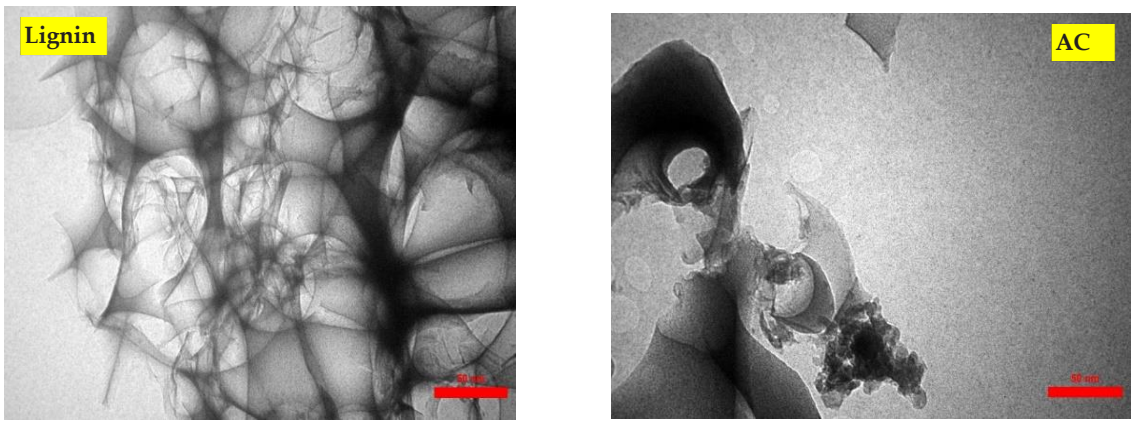

Fig. 8. TEM results of lignin and AC.

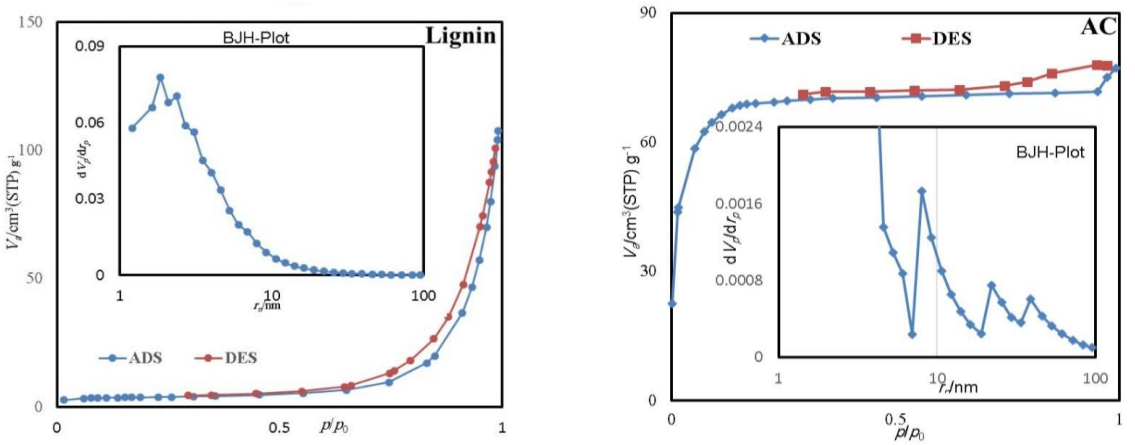

Fig. 9. BET plots of lignin and AC.

Table 1. BET surface area and pore structure of lignin and AC samples.

Physicochemical properties	Lignin	AC
BET surface area, m²/g	31.632	270.42
BJH surface area, m²/g	11.08	28.032
Pore Volume, cm³/g	22.125	48.841
Mean pore diameter, nm	0.8756	1.6905
Isotherm type	III	III
hysteresis loop	H3	H3

with incremental amounts of K_2CO_3 promoted the formation of micropores, leading to products with larger surface area and pore volume. However, study revealed that the excessive impregnation ratios and activation temperatures can cause pore widening and burn-off [52, 60].

Adsorption of CR dye onto AC

Effect of contact time

A rapid uptake of pollutants and establishment of equilibrium within a short timeframe is an indication of adsorbent's efficiency for water treatment. The adsorption of CR dye onto AC was evaluated under controlled experimental conditions, including a time range of 0-45 minutes, an adsorbent dose of 0.01 g/ 25 ml, at the pH of 7 and temperature of 25 °C. The initial CR dye concentration was 50 mg/l. The contact time was maintained at 45 minutes, with a constant stirring velocity of 110 rpm. The absorbance of the mixtures was analyzed using a UV-Vis spectrophotometer (Shimadzu, Japan) at a maximum wavelength (λ_{max}) of 498 nm for CR dye. Fig. 10 showed that adsorption of CR dye onto AC increased with time until it gradually reached equilibrium. The adsorption process can be divided into three distinct stages. In the first stage, a rapid initial adsorption was observed due to the concentration gradient of CR dye between solution and surface of AC. Simultaneously, AC possesses a sufficient number of active sites, enabling a rapid increase in amount of adsorbed CR dye. In the second stage, however, the adsorption rate decreases as active sites on activated carbon surface become progressively occupied by dye molecules. The concentration gradient between the solution and adsorbent also diminishes due to repulsive interactions, making it more difficult for additional CR dye molecules to bind to active sites. In third stage of adsorption, all active sites are completely occupied, rendering further adsorption challenging. As a result, equilibrium is reached, and optimum contact time for this process is determined to be 20 min, corresponding to a removal efficiency of 70.21% [61-63].

Effect of adsorbent dosage and dye concentration

The adsorbent dose significantly affects the adsorption process by determining the adsorbent-adsorbate equilibrium within the system. The quantity of adsorbent directly relates to the number of available adsorption sites, which, in turn, affect removal efficiency. To investigate the effect of adsorbent dose on adsorption capacity, experiments were conducted using varying amounts of adsorbent (0.001-0.009 g/l)

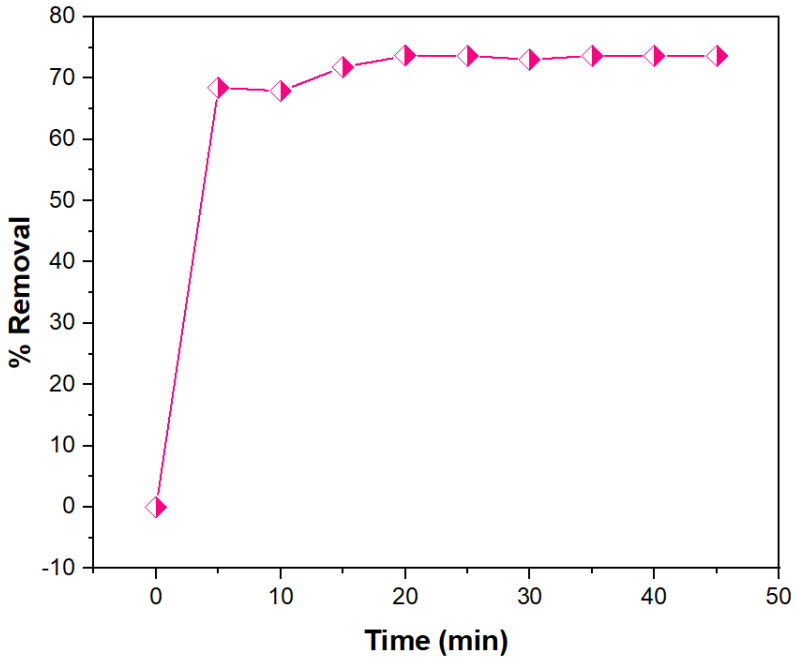

Fig. 10. Effect of contact time on adsorption efficiency of AC towards CR dye.

under optimal conditions (for 20 min at pH 7 and temperature of 25 °C). As depicted in Fig. 11 (left), increasing the AC dosage from 0.001 g/l to 0.007 g/l led to a corresponding increase in removal efficiency from 43.427 % to 68.553 %. This enhancement is attributed to the increased availability of active sites on adsorbent surface. However, further increasing the adsorbent dose beyond 0.007 g/l did not result in a significant increase in adsorption capacity. This saturation point suggests that the active sites on adsorbent surface become saturated, limiting additional adsorption [55, 64]. The results of the dye concentration on CR dye adsorption shown in Fig. 11 (right) highlight the continuous increase in adsorption capacity with an increase of dye concentration. With the increase in initial dye concentration from 10 mg/l to 50 mg/l, there was a continuous increase in adsorption capacity from 35.04 mg/g to 160.60 mg/g respectively. This behavior can be attributed to the increase in interaction between adsorbent surface and the dye molecules with continuous increase in dye concentration. These thereby results in increasing the adsorption of CR dye molecules on the surface of AC [65].

Effect of pH

The pH of aqueous solutions significantly affects the adsorption process by influencing the surface charge of adsorbent and degree of ionization of adsorbate, thereby impacting the adsorption mechanism [66-68]. To investigate the effect of initial pH on adsorption efficiency, experiments were conducted at pH values of 4, 6, 8, and 10 under optimal conditions (i.e., using adsorbent

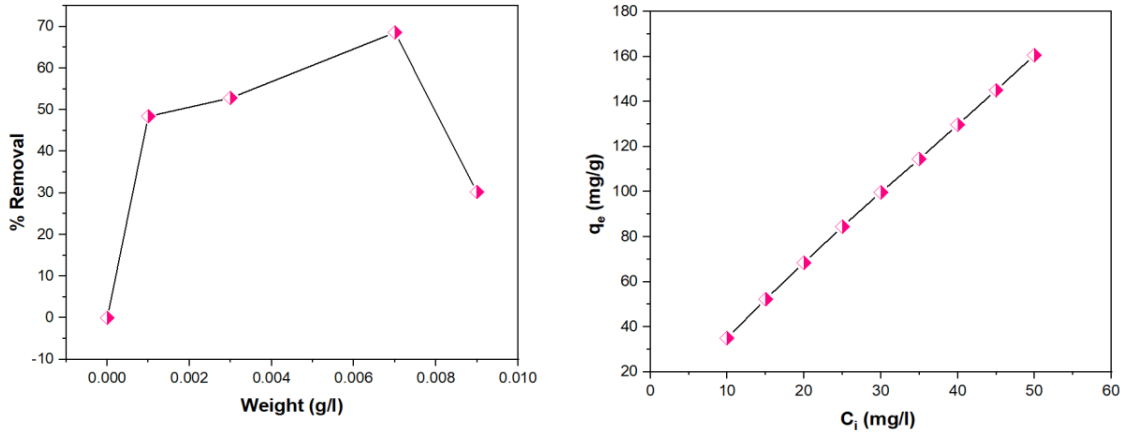

Fig. 11. Effect of (left) adsorbent weight and (right) dye concentration on adsorption efficiency of AC towards CR dye.

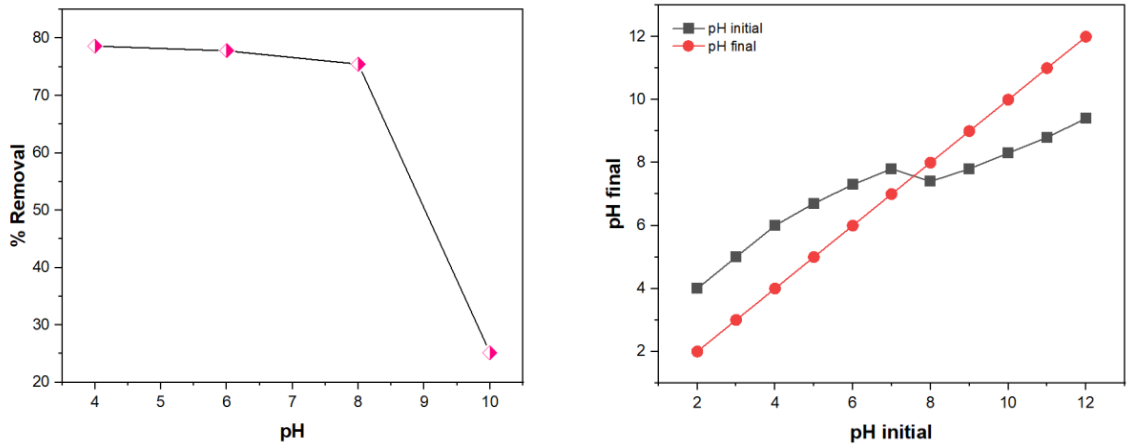

Fig. 12. Effect of pH (left), pH_{zpc} (right) on adsorption efficiency for CR dye.

dose of 0.007 g/l for the contact time of 20 min using dye concentration of 50 mg/l at 25 °C). As shown in Fig. 12 (left), the maximum removal of CR dye (78.616%) was achieved at pH 4. At lower pH values, the uptake of CR dye, an anionic dye, is attributed to the interaction between acidic medium and dye. Conversely, at higher pH values, the increasing concentration of hydroxyl groups in basic medium leads to an increase in negative charges on both dye and adsorbent surface. This electrostatic repulsion between similarly charged species results in a decrease in removal efficiency, with only 25.157% removal observed at pH 10. The point of zero charge (pH_{pzc}) is a critical parameter that determines the pH sensitivity range and indicates the type of active sites on adsorbent surface. Anionic dye adsorption is favoured at pH values below pH_{pzc} when the surface is positively charged, while cationic dye adsorption is favoured at pH values above pH_{pzc} due to presence of negative functional groups such as OH^-. As illustrated in Fig. 12 (right), the pH_{pzc} for AC was found to be 7.8. Below this value, the increased concentration of H^+ ions in dye solution leads to a more acidic environment, resulting in a positively charged adsorbent surface and enhanced electrostatic attraction with anionic dye. Conversely, pH values above pH_{pzc} lead to an increase in OH^- ion concentration, resulting in a negatively charged adsorbent surface and reduced adsorption capacity due to electrostatic repulsion between similar charges.

Effect of temperature and adsorption thermodynamic

Temperature is a critical parameter influencing adsorption capacity and overall adsorption process. To investigate the effect of temperature on uptake of CR dye by AC, experiments were conducted at temperatures ranging from 293 K to 308 K for 20 min. As shown in Fig. 13 (left), increasing temperature favoured the transport of adsorbate into pores of AC, leading to an increase in the amount of CR dye adsorbed by AC and removal efficiency from 77.98 % to 89.93 % as temperature increased from 20 °C to 35 °C. The enhanced adsorption capacity at higher temperatures can be attributed to both the decreased solubility of CR dye and increased molecular movement, enabling the dye molecules to interact more effectively with active sites on adsorbent surface. A thermodynamic study conducted over

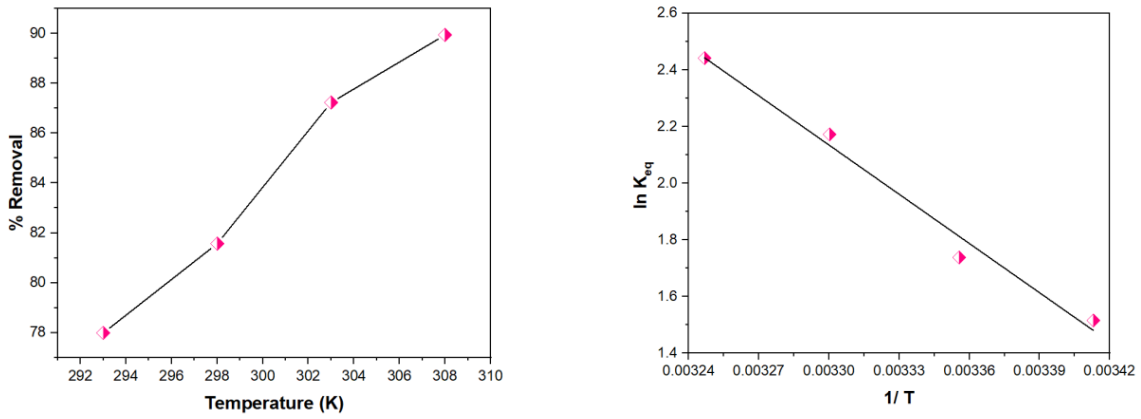

Fig. 13. Effect of temperature on CR dye adsorption by AC (left), variation of ln K_e as a function of 1/T (right).

Table 2. Thermodynamic values of adsorption CR dye on AC.

System	Temp. (K)	-ΔG (kJ/mol)	ΔH (kJ/mol)	ΔS (J/mol K)	ln Keq
CR/AC	293	-3.69358	41.4112	153.9412	1.51624
	298	-4.30838		153.4214	1.73895
	303	-5.47411		154.7370	2.17300
	308	-6.25216		154.7512	2.44157

temperature range of 20-35°C provided insights into nature of adsorption process and the degree of freedom of dye molecules. Thermodynamic parameters such as enthalpy change (ΔH), entropy change (ΔS), and Gibbs free energy change (ΔG) were calculated using Eqs. 5-8 [69] and results are presented in Table 2.

$$K_{eq} = \frac{Q_e \times V}{C_e \times m} \quad (5)$$

$$\Delta G = - RT \ln k_{eq} \quad (6)$$

$$Lnk_{eq} = \frac{\Delta S}{R} - \frac{\Delta H}{RT} \quad (7)$$

$$\Delta G = \Delta H - T\Delta S \quad (8)$$

Where k_{eq}, is thermodynamic equilibrium constant, Q_e is amount of dye adsorbed in solution (mg/g), C_e is equilibrium concentration of dye solution (mg/l), R is universal gas constant (8.314 J/ mol.K) and T is temperature in Kelvin. The values of ΔH and ΔS were determined from intercept and slope of plot shown in Fig. 13 (right), respectively. The results indicate that adsorption capacity increases with increasing temperature, suggesting an endothermic nature of adsorption process. Furthermore, the positive value of ΔH supports these results. Additionally, the positive value of ΔS suggests a higher degree of freedom for molecules in adsorbed phase compared to liquid phase, indicating increased randomness at solid-liquid interface. In contrast, negative values of ΔG at all temperatures clearly highlights that adsorption of CR dye onto adsorbent is feasible and spontaneous. The obtained thermodynamic values are summarized in Table 2.

Adsorption isotherm studies

To assess the applicability of adsorption for removing CR dye from aqueous solutions using AC, several commonly used isotherm models, including Langmuir, Freundlich, and Temkin, were employed.

Langmuir isotherm

The Langmuir isotherm is applicable to solid-

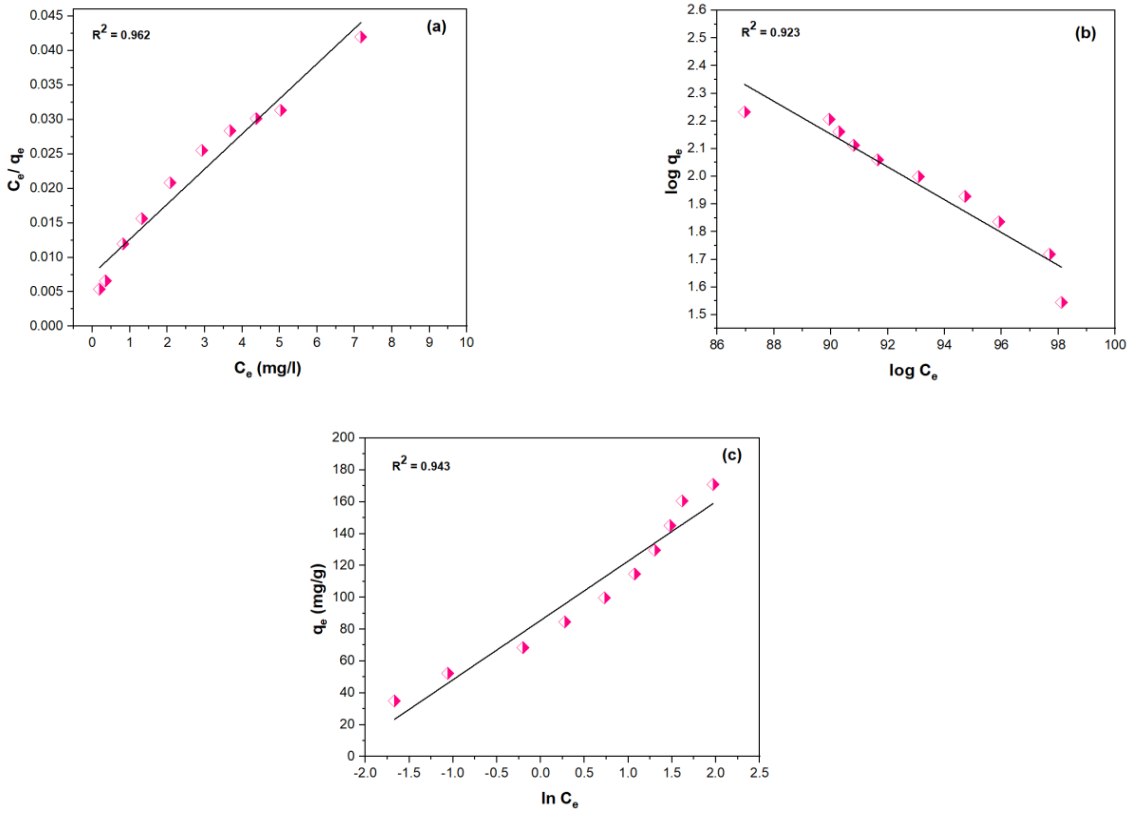

Fig. 14. Plot of (a) Langmuir isotherm, (b) Freundlich isotherm and (c) Temkin isotherm models.

liquid systems and postulates that adsorption occurs at specific, homogeneous monolayer sites on adsorbent. It assumes that all active sites on surface have identical adsorption energies and adsorbate is distributed equally among these sites. The nonlinear and linearized forms of the Langmuir isotherm equation are as follows:

$$q_e = \frac{q_m k_L C_e}{1+k_L C_e} \quad (9)$$

$$\frac{C_e}{q_e} = \frac{C_e}{q_m} + \frac{1}{b \times q_m} \quad (10)$$

here, q_e is amount of dye adsorbed on unit mass of adsorbent at equilibrium (mg/g), q_{max} is maximum quantity of adsorbate to form monolayer adsorption capacity (mg/g), C_e is equilibrium dye concentration in solution (mg/l), b is Langmuir isotherm constant attributed to affinity of binding sites (l/mg). The parameter q_m can be calculated from slope of linear plot of C_e/ q_m versus C_e. The most important feature of Langmuir isotherm can be made on basis of a dimensionless constant R_L, which is known as separation factor or equilibrium parameter and expressed as:

$$R_L = \frac{1}{(1+b\, C_0)} \quad (11)$$

here, C_o represents initial concentration of CR dye (mg/l). R_L values indicate the shape of isotherm. If its value ranges between 0 and 1, the adsorption process is considered as favourable ($0 < R_L \leq 1$). When R_L equates unity, the process is linear and irreversible. If R_L is greater than 1 ($R_L > 1$), the adsorption is unfavourable [70-72]. Fig. 14a and Table 3 present the results of Langmuir isotherm for CR dye. The experimental R_L value of 0.0180 indicates a good fit to the Langmuir isotherm model, consistent with the requirements for favourable adsorption.

Freundlich isotherm

The Freundlich isotherm model is applicable for non-ideal adsorption and is an empirical equation used to describe heterogeneous surfaces of adsorbents and multilayer adsorption. This model accounts for distribution of active sites on adsorbent surface and interactions between adsorbed molecules. The nonlinear form of the Freundlich equation can be expressed as below:

$$Q_e = k_F\, C_e^{\frac{1}{n}} \quad (12)$$

In Freundlich isotherm model, is a constant representing the adsorption capacity, while 1/n refers to the adsorption intensity. The value of 1/n varies with the heterogeneity of material, and n reflects the mutual interaction between adsorbed species. Q_m represents the equilibrium adsorption capacity (mg/g), and C_e is equilibrium dye concentration (mg/l). The linear form of the Freundlich isotherm is represented by following equation [73]:

$$\log Q_e = \log k_F + \frac{1}{n} \log C_e \quad (13)$$

The values of k_F and 1/n were obtained from intercept and slope of a straight-line plot of log Q_e versus log C_e. The applicability of the isotherm equations was compared using correlation coefficient (R^2). Fig. 14b and Table 3 show the results of Freundlich model revealing the better

Table 3. Langmuir, Freundlich and Temkin model parameters calculated for adsorption of CR dye on AC.

Isotherm model	Parameters	Values
Langmuir	q_m (mg/g)	196.0784
	b (L/mg)	1.08974
	R_L	0.018022
	R^2	0.96200
Freundlich	k_F (mg/g)	3.03528
	n	16.8919
	R^2	0.9233
Temkin	k_T (L/mg)	1.44
	B	37.245
	R^2	0.9433

fit to Langmuir model compared to Freundlich model. These results suggest a homogeneous nature of the AC surface and formation of a monolayer of CR dye molecules on its exterior surface. Furthermore, the value of 1/n indicates the favourability of adsorption process. A value of n close to zero suggests a more heterogeneous system. The experimental values of n are greater than 1 (n > 1), indicating repulsive forces between adsorbed molecules and favourable adsorption conditions.

Temkin isotherm

The Temkin model is used for heterogeneous surface systems with non-uniform adsorption heat distributions. This model assumes a linear decrease in heat of adsorption for all molecules in layer with low interactions taking place between studied adsorbent and adsorbate. The linear form of the Temkin isotherm is represented by the following equation [73, 74]:

$$q_e = B\ln k_T + B\ln C_e \quad (14)$$

here, B refers to Temkin constant that is related to heat of adsorption (J/ mol), R = universal gas constant (8.314J/ mol.K), T = absolute temperature (K), b = Temkin isotherm constant, k_T = Temkin isotherm equilibrium binding constant (l/mg) corresponding to maximum binding energy. Values B and k_T can be calculated from slope and intercept of graph (q_e versus log C_e) respectively. Fig. 14c shows the Temkin isotherm model and parameters calculated from this model are listed in Table 3. Results revealed that the best fit for CR dye was obtained with Langmuir revealing the R^2 of 0.9620 followed by Temkin showing R^2 of 0.9433 and Freundlich with R^2 of 0.9233.

In adsorption, molecules within the bulk material experience cohesive forces of equal magnetic magnitude in all directions. However, molecules on surface are pulled downwards and sideways. When the opportunity of adsorption increases, surface atoms or molecules will attempt to satisfy their unsaturated valence by bonding with other molecules or atoms. This bonding reduces surface energy. If the bonding occurs primarily through Van der Waals forces, the adsorption is known as physisorption. If the surface is unsaturated, chemical forces take place, leading to bond formation and chemisorption. This phenomenon is in good agreement with Langmuir

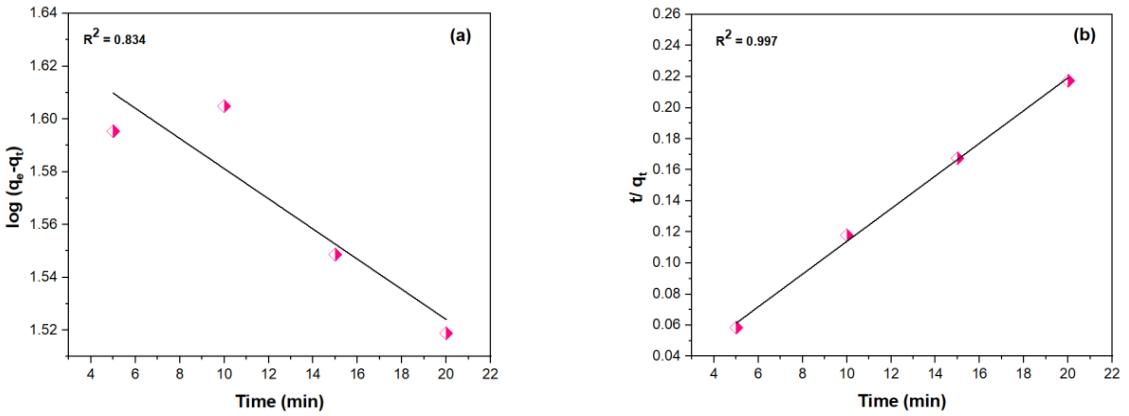

Fig. 15. Kinetic plot for (a) pseudo–first order and (b) pseudo–second order for adsorption of CR dye on AC.

Table 4. Values of kinetic parameters for adsorption of CR on AC.

Model	Parameters		
Pseudo-first order	k_1	q_e	R^2
	0.04606	0.86178	0.834
Pseudo-second order	k_2	q_e	R^2
	0.1681	121.9512	0.997

isotherm.

Adsorption kinetics

Kinetic studies elucidate the rate and mechanism of adsorption process. Solid-liquid adsorption processes on porous surfaces often involve multiple steps. Initially, the external mass of adsorbate transfers from liquid phase (solution) to solid surface through boundary layer. Subsequently, internal diffusion occurs within porous particles of adsorbent, followed by adsorption onto adsorbent surface. Based on adsorptive behaviours and potential rate-controlling mass transport and chemical reaction processes, adsorption kinetics were investigated using two kinetic models namely the Lagergren pseudo-first-order and pseudo-second-order models. The pseudo-first-order model is concerned with the physical forces between adsorbent and adsorbate and assumes that adsorption rate is proportional to unoccupied sites on adsorbent surface [75-79]. The pseudo-first order equation, is shown in Eq. 15 as below:

$$\mathrm{Log}\,(q_e - q_t) = \log q_e - \left(\frac{k_1}{2.303}\right) x\, t \qquad (15)$$

The constant reaction rate k_1 (min^{-1}) can be determined from the slope of the (q_e-q_t) versus t plot. Here, q_e represents equilibrium adsorption capacity (mg/g), q_t represents amount of dye adsorbed at time t (mg/g), and k_1 refers to adsorption rate constant (min^{-1}).

The pseudo–second order kinetic equation, is represented by Eq. 16:

$$\frac{t}{q_t} = \frac{1}{q_e} + \frac{1}{k_2 q_e^2} \qquad (16)$$

The constant reaction rate k_2 (g/mg·min) and q_e are calculated from slope and intercept of straight-line plot of t/q_t versus t, respectively. The kinetic study of CR dye removal on AC at equilibrium contact time revealed the characteristics of adsorption behaviour. Both pseudo-first-order and pseudo-second-order models were applied to experimental data obtained, as shown in Fig. 15a and b. The results, reported in Table 4, indicate correlation values of R^2 = 0.834 for pseudo-first-order model and R^2 = 0.997 for pseudo-second-order model. The higher correlation coefficient for pseudo-second-order model suggests a better fit to adsorption data than pseudo-first-order model. Additionally, the equilibrium adsorption capacity for pseudo-first-order model was found to be 0.861, which is significantly lower than qe value of 121.951 for pseudo-second-order model. This suggests that pseudo-second-order model is in close agreement with experimental data and implies that rate-limiting step is chemisorption-type, indicating an adsorption mechanism related to adsorbent and adsorbate.

CONCLUSION

This study demonstrates the preparation of activated carbon (AC) with high porosity and specific surface area from agricultural waste lignin derived from straw pulping. Activation using K_2CO_3 as an activating agent and varying impregnation ratios affects yield of nano activated carbon. Activation time and carbonization temperature also play substantial roles in product quantity. The raw material and AC were characterized using various techniques. The efficiency of AC as an adsorbent was evaluated for removal of congo red (CR) dye from aqueous solutions. The adsorption process was influenced by experimental conditions such as contact time, adsorbent dose, pH, and temperature. The highest percentage removal of CR dye by AC under optimal conditions was 89.9375%. Thermodynamic studies revealed that adsorption of CR dye is endothermic and spontaneous. The Langmuir isotherm model provided best fit for CR adsorption, and kinetic study results indicated that adsorption of CR dye follows pseudo-second-order model. The findings of this work suggest that nano lignin-based carbon materials can be utilized as eco-friendly and low-cost adsorbent for adsorption of dyes.

CONFLICT OF INTEREST

The authors declare that there is no conflict of interests regarding the publication of this manuscript.

REFERENCES

1. Shah A, Arjunan A, Baroutaji A, Zakharova J. A review of physicochemical and biological contaminants in drinking water and their impacts on human health. Water Science and Engineering. 2023;16(4):333-344.
2. Guo X, Zhang S, Shan X-q. Adsorption of metal ions on lignin. J Hazard Mater. 2008;151(1):134-142.
3. Bedmohata M.A# Chaudhari A.R. Singh S.P. Chaudhari M.D BMACARSSPCMD. Preparation of activated carbon from industrial waste lignin by chemical activation. International Journal of Researches in Biosciences and Agriculture Technology. 2014.
4. Paul S, Bhardwaj SK, Kaur R, Bhaumik J. Lignin-Derived

Hybrid Materials as Promising Adsorbents for the Separation of Pollutants. ACS Symposium Series: American Chemical Society; 2020. p. 225-261.
5. Batool M, Javed T, Wasim M, Zafar S, Din MI. Exploring the usability of Cedrus deodara sawdust for decontamination of wastewater containing crystal violet dye. Desalination and Water Treatment. 2021;224:433-448.
6. Ghzal Q, Javed T, Batool M. Potential of easily prepared low-cost rice husk biochar and burnt clay composite for the removal of methylene blue dye from contaminated water. Environmental Science: Water Research and Technology. 2023;9(11):2925-2941.
7. Mannan HA, Nadeem R, Bibi S, Javed T, Javed I, Nazir A, et al. Mesoporous activated TiO_2 /based biochar synthesized from fish scales as a proficient adsorbent for deracination of heavy metals from industrial efflux. Journal of Dispersion Science and Technology. 2022;45(2):329-341.
8. Shah A, Arjunan A, Thumma A, Zakharova J, Bolarinwa T, Devi S, et al. Adsorptive removal of arsenic from drinking water using KOH-modified sewage sludge-derived biochar. Cleaner Water. 2024;2:100022.
9. Shah A, Zakharova J, Batool M, Coley MP, Arjunan A, Hawkins AJ, et al. Removal of cadmium and zinc from water using sewage sludge-derived biochar. Sustainable Chemistry for the Environment. 2024;6:100118.
10. Arshad R, Javed T, Thumma A. Exploring the efficiency of sodium alginate beads and Cedrus deodara sawdust for adsorptive removal of crystal violet dye. Journal of Dispersion Science and Technology. 2023;45(12):2330-2343.
11. Javed T, Thumma A, Uddin AN, Akhter R, Babar Taj M, Zafar S, et al. Batch adsorption study of Congo Red dye using unmodified Azadirachta indica leaves: isotherms and kinetics. Water Practice and Technology. 2024;19(2):546-566.
12. Rehman H, Javed T, Thumma A, Uddin AN, Singh N, Baig MM, et al. Potential of easily available low-cost raw cotton for the elimination of methylene blue dye from polluted water. Desalination and Water Treatment. 2024;318:100319.
13. Bukhari A, Javed T, Haider MN. Adsorptive exclusion of crystal violet dye from wastewater by using fish scales as an adsorbent. Journal of Dispersion Science and Technology. 2022;44(11):2081-2092.
14. Imran MS, Javed T, Areej I, Haider MN. Sequestration of crystal violet dye from wastewater using low-cost coconut husk as a potential adsorbent. Water Sci Technol. 2022;85(8):2295-2317.
15. Urooj H, Javed T, Taj MB, Nouman Haider M. Adsorption of crystal violet dye from wastewater on Phyllanthus emblica fruit (PEF) powder: kinetic and thermodynamic. Int J Environ Anal Chem. 2023:1-26.
16. Shah A, Arjunan A, Manning G, Batool M, Zakharova J, Hawkins AJ, et al. Sequential novel use of Moringa oleifera Lam., biochar, and sand to remove turbidity, E. coli, and heavy metals from drinking water. Cleaner Water. 2024;2:100050.
17. Shokoohi R, Samadi MT, Amani M, Poureshgh Y. Optimizing laccase-mediated amoxicillin removal by the use of Box–Behnken design in an aqueous solution. Desalination and Water Treatment. 2018;119:53-63.
18. Shokoohi R, Samadi MT, Amani M, Poureshgh Y. Modeling and optimization of removal of cefalexin from aquatic solutions by enzymatic oxidation using experimental design. Brazilian Journal of Chemical Engineering. 2018;35(3):943-956.
19. Zafar MN, Dar Q, Nawaz F, Zafar MN, Iqbal M, Nazar MF. Effective adsorptive removal of azo dyes over spherical ZnO nanoparticles. Journal of Materials Research and Technology. 2019;8(1):713-725.
20. Albadarin AB, Collins MN, Naushad M, Shirazian S, Walker G, Mangwandi C. Activated lignin-chitosan extruded blends for efficient adsorption of methylene blue. Chem Eng J. 2017;307:264-272.
21. Litefti K, Freire MS, Stitou M, González-Álvarez J. Adsorption of an anionic dye (Congo red) from aqueous solutions by pine bark. Sci Rep. 2019;9(1).
22. Atyaa AI, Radhy ND, Jasim LS. Synthesis and Characterization of Graphene Oxide/Hydrogel Composites and Their Applications to Adsorptive Removal Congo Red from Aqueous Solution. Journal of Physics: Conference Series. 2019;1234(1):012095.
23. Bayramov A. Environmental Regionalism in the Caspian Sea: A Functionalist Approach. Globalizing Regionalism and International Relations: Policy Press; 2021. p. 103-124.
24. Ahmad MA, Herawan SG, Yusof AA. Effect of Activation Time on the Pinang Frond based Activated Carbon for Remazol Brilliant Blue R Removal. Journal of Mechanical Engineering and Sciences. 2014;7:1085-1093.
25. Acut E, Anorico NF, Acut D. Optimization of the Removal of Hexavalent Chromium Cr(VI) from Aqueous Solution by Moringa oleifera Bark-Derived Activated Carbon (MOBAC) Using Response Surface Methodology (RSM). Orbital: The Electronic Journal of Chemistry. 2023:186-197.
26. Li W, Zhang Y, Das L, Wang Y, Li M, Wanninayake N, et al. Linking lignin source with structural and electrochemical properties of lignin-derived carbon materials. RSC Advances. 2018;8(68):38721-38732.
27. Lahti R, Bergna D, Romar H, Hu T, Comazzi A, Pirola C, et al. Characterization of Cobalt Catalysts on Biomass-Derived Carbon Supports. Topics in Catalysis. 2017;60(17-18):1415-1428.
28. Bergna D, Varila T, Romar H, Lassi U. Activated carbon from hydrolysis lignin: Effect of activation method on carbon properties. Biomass Bioenergy. 2022;159:106387.
29. Jin XJ, Yu ZM, Yan GJ, Yu W. Preparation of Activated Carbon of Lignin from Straw Pulping by Chemical Activation Using Potassium Carbonate. Materials Science Forum. 2011;704-705:517-522.
30. Williams P, Reed A. Development of activated carbon pore structure via physical and chemical activation of biomass fibre waste. Biomass Bioenergy. 2006;30(2):144-152.
31. Elewa AM, Amer AA, Attallah MF, Gad HA, Al-Ahmed ZAM, Ahmed IA. Chemically Activated Carbon Based on Biomass for Adsorption of Fe(III) and Mn(II) Ions from Aqueous Solution. Materials. 2023;16(3):1251.
32. Shah A, Arjunan A, Manning G, Zakharova J, Andraulaki I, Batool M. The effect of dose, settling time, shelf life, storage temperature and extractant on Moringa oleifera Lam. protein coagulation efficiency. Environmental Nanotechnology, Monitoring and Management. 2024;21:100919.
33. Louarrat M, Enaime G, Baçaoui A, Yaacoubi A, Blin J, Martin L. Optimization of conditions for the preparation of activated carbon from olive stones for application in gold recovery. Journal of the Southern African Institute of Mining and Metallurgy. 2019;119(3).
34. Khan SA, Khan SB, Khan LU, Farooq A, Akhtar K, Asiri AM. Fourier Transform Infrared Spectroscopy: Fundamentals and Application in Functional Groups and Nanomaterials Characterization. Handbook of Materials Characterization:

Springer International Publishing; 2018. p. 317-344.
35. Zainal NH. Carbonisation-activation of oil palm kernel shell to produce activated carbon and methylene blue adsorption kinetics. Journal of Oil Palm Research. 2018.
36. Geçgel Ü, Üner O, Gökara G, Bayrak Y. Adsorption of cationic dyes on activated carbon obtained from waste Elaeagnus stone. Adsorption Science and Technology. 2016;34(9-10):512-525.
37. Harimisa GE, Jusoh NWC, Tan LS, Shameli K, Ghafar NA, Masudi A. Synthesis of potassium hydroxide-treated activated carbon via one-step activation method. Journal of Physics: Conference Series. 2022;2259(1):012009.
38. Mussatto SI, Fernandes M, Rocha GJM, Órfão JJM, Teixeira JA, Roberto IC. Production, characterization and application of activated carbon from brewer's spent grain lignin. Bioresour Technol. 2010;101(7):2450-2457.
39. Kim J-H, Lee G, Park J-E, Kim S-H. Limitation of K_2CO_3 as a Chemical Agent for Upgrading Activated Carbon. Processes. 2021;9(6):1000.
40. Nagalakshmi TV, Emmanuel KA, Suresh Babu C, Chakrapani C, Divakar PP. Preparation of Mesoporous Activated Carbon from Jackfruit PPI-1 Waste and Development of Different Surface Functional Groups. International Letters of Chemistry, Physics and Astronomy. 2015;54:189-200.
41. Suhas, Carrott PJM, Ribeiro Carrott MML. Lignin – from natural adsorbent to activated carbon: A review. Bioresour Technol. 2007;98(12):2301-2312.
42. Kareem NS, Mohammed SA, Abed MJ, Aneed AH, Kamal HM, Zahid NI, et al. New macrocycles incorporating glycolipids via copper-catalyzed triazole coupling. J Carbohydr Chem. 2022;41(1):1-17.
43. Razavi FS, Mahdi MA, Ghanbari D, Dawi EA, Abed MJ, Ganduh SH, et al. Fabrication and design of four-component Bi_2S_3/$CuFe_2O_4$/CuO/Cu_2O nanocomposite as new active materials for high performance electrochemical hydrogen storage application. Journal of Energy Storage. 2024;94:112493.
44. Bayati-Komitaki N, Ganduh SH, Alzaidy AH, Salavati-Niasari M. A comprehensive review of Co_3O nanostructures in cancer: Synthesis, characterization, reactive oxygen species mechanisms, and therapeutic applications. Biomedicine and Pharmacotherapy. 2024;180:117457.
45. Jamdar M, Monsef R, Ganduh SH, Dawi EA, Jasim LS, Salavati-Niasari M. Unraveling the potential of sonochemically achieved $DyMnO_3$/Dy_2O_3 nanocomposites as highly efficient visible-light-driven photocatalysts in decolorization of organic contamination. Ecotoxicology and Environmental Safety. 2024;269:115801.
46. Majeed HJ, Idrees TJ, Mahdi MA, Abed MJ, Batool M, Yousefi SR, et al. Synthesis and application of novel sodium carboxy methyl cellulose-g-poly acrylic acid carbon dots hydrogel nanocomposite (NaCMC-g-PAAc/ CDs) for adsorptive removal of malachite green dye. Desalination and Water Treatment. 2024;320:100822.
47. Batool M, Haider MN, Javed T. Applications of Spectroscopic Techniques for Characterization of Polymer Nanocomposite: A Review. Journal of Inorganic and Organometallic Polymers and Materials. 2022;32(12):4478-4503.
48. Shukla AK, Alam J, Ruokolainen J, Kesari KK. Biopolymer Chitosan-Activated Charcoal Adsorptive Composite Material: A Feasible Approach to Methylene Blue Dye Removal from Water. MDPI AG; 2023.
49. Halysh V, Skiba M, Nesterenko A, Kulik T, Palianytsia B. Structural characterization of by-product lignins from organosolv rapeseed straw pulping and their application as biosorbents. Journal of Polymer Research. 2022;29(12).
50. da Silva Lacerda V, López-Sotelo JB, Correa-Guimarães A, Hernández-Navarro S, Sánchez-Báscones M, Navas-Gracia LM, et al. Rhodamine B removal with activated carbons obtained from lignocellulosic waste. J Environ Manage. 2015;155:67-76.
51. Rao HJ. Characterization Studies on Adsorption of Lead and Cadmium Using Activated Carbon Prepared from Waste Tyres. Nature Environment and Pollution Technology. 2021;20(2).
52. Garba A, Basri H, Nasri NS. Preparation and Characterization of Green Porous Palm Shell Based Activated Carbon by Two Step Chemical Activation Using KOH. Applied Mechanics and Materials. 2015;773-774:1127-1132.
53. Li X-f, Luo X-g, Dou L-q, Chen K. Preparation and Characterization of K_2CO_3-Activated Kraft Lignin Carbon. BioResources. 2016;11(1).
54. Ghaffar SH, Fan M. Structural analysis for lignin characteristics in biomass straw. Biomass Bioenergy. 2013;57:264-279.
55. Adegoke HI, Adekola FA, Olowookere IT, Yaqub AL. Thermodynamic studies on adsorption of lead (II) Ion from aqueous solution using magnetite, activated carbon and composites. Journal of Applied Sciences and Environmental Management. 2017;21(3):440.
56. Osman AI, Blewitt J, Abu-Dahrieh JK, Farrell C, Al-Muhtaseb AaH, Harrison J, et al. Production and characterisation of activated carbon and carbon nanotubes from potato peel waste and their application in heavy metal removal. Environmental Science and Pollution Research. 2019;26(36):37228-37241.
57. Han W, Luo L, Zhang S. Adsorption of bisphenol A on lignin: effects of solution chemistry. Int J Environ Sci Technol (Tehran). 2012;9(3):543-548.
58. Fromm J, Rockel B, Lautner S, Windeisen E, Wanner G. Lignin distribution in wood cell walls determined by TEM and backscattered SEM techniques. J Struct Biol. 2003;143(1):77-84.
59. Kayiwa R, Kasedde H, Lubwama M, Kirabira JB. Mesoporous activated carbon yielded from pre-leached cassava peels. Research Square Platform LLC; 2021.
60. Chen R, Li L, Liu Z, Lu M, Wang C, Li H, et al. Preparation and characterization of activated carbons from tobacco stem by chemical activation. Journal of the Air and Waste Management Association. 2017;67(6):713-724.
61. Abbas M, Trari M. Kinetic, equilibrium and thermodynamic study on the removal of Congo Red from aqueous solutions by adsorption onto apricot stone. Process Saf Environ Prot. 2015;98:424-436.
62. Hanum L, Adlim M, Anita, Rahmayani RFI, Nazar M, Puspita K. The adsorption capacity of methylene blue by activated carbon immobilized yarn. RASAYAN Journal of Chemistry. 2022;15(03):1965-1974.
63. Yang J, Li C, Yang B, Kang S, Zhang Z. Study on Adsorption of Chromium (VI) by Activated Carbon from Cassava Sludge. IOP Conference Series: Earth and Environmental Science. 2018;128:012017.
64. Hevea brasiliensis (Rubber Seed) Oil: Extraction, Characterization, and Kinetics of Thermo-oxidative Degradation Using Classical Chemical Methods. American Chemical Society (ACS).
65. Zheng Y, Zhang J, Wang A. Fast removal of ammonium nitrogen from aqueous solution using chitosan-g-poly(acrylic acid)/attapulgite composite. Chem Eng J. 2009;155(1-2):215-222.

66. Wang P, Yan T, Wang L. Removal of Congo Red from Aqueous Solution Using Magnetic Chitosan Composite Microparticles. BioResources. 2013;8(4).
67. Shafiqul Alam M. Removal of Congo Red Dye from Industrial Wastewater by Untreated Sawdust. American Journal of Environmental Protection. 2015;4(5):207.
68. Abbas A, Rehman R, Murtza S, Ayub R. Isothermal Evaluation of Chemical Modification of Ricinus communis Stem Used for Adsorptive Removal of Brilliant Blue FCF Dye from Water. Asian J Chem. 2013;25(16):9153-9158.
69. Removal of Congo Red Dye using Activated Carbon Developed from Bio-waste. BCAEBS-19 and LBGIS-19 July 22-24, 2019 Budapest (Hungary); 2019/07/22: Emirates Research Publishing; 2019.
70. Joshi S, Pokharel BP. Preparation and Characterization of Activated Carbon from Lapsi (Choerospondias axillaris) Seed Stone by Chemical Activation with Potassium Hydroxide. Journal of the Institute of Engineering. 2014;9(1):79-88.
71. Wanyonyi WC, Onyari JM, Shiundu PM. Adsorption of Congo Red Dye from Aqueous Solutions Using Roots of Eichhornia Crassipes: Kinetic and Equilibrium Studies. Energy Procedia. 2014;50:862-869.
72. TekİN B, AÇIkel U. Adsorption Isotherms for Removal of Heavy Metal Ions (Copper and Nickel) from Aqueous Solutions in Single and Binary Adsorption Processes. Gazi University Journal of Science. 2023;36(2):495-509.
73. Pascu D-E, Pascu M, Traistaru GA, Nechifor AC, Miron AR. Iron and manganese removal from drinking water. Journal of Electrochemical Science and Engineering. 2015;0(0).
74. Rouf S, Nagapadma M. Chitosan and Surfactant Impregnated Chitosan Beads for Removal of Textile Dye Brilliant Black BN from Aqueous Solution. International Journal of Scientific and Engineering Research. 2015;6(1):1268-1275.
75. Priyadarshini B, Rath PP, Behera SS, Panda SR, Sahoo TR, Parhi PK. Kinetics, Thermodynamics and Isotherm studies on Adsorption of Eriochrome Black-T from aqueous solution using Rutile TiO_2. IOP Conference Series: Materials Science and Engineering. 2018;310:012051.
76. Khan A, Malik A, Humayun M, Shah N, Ismail M, Yahia M, et al. Improvement of the adsorption efficiency of rice husk ash for crystal violet dye removal from aqueous medium. Egyptian Journal of Chemistry. 2022;0(0):0-0.
77. Cotoruelo LM, Marqués MD, Díaz FJ, Rodríguez-Mirasol J, Rodríguez JJ, Cordero T. Adsorbent ability of lignin-based activated carbons for the removal of p-nitrophenol from aqueous solutions. Chem Eng J. 2012;184:176-183.
78. Erhayem M, Al-Tohami F, Mohamed R, Ahmida K. Isotherm, Kinetic and Thermodynamic Studies for the Sorption of Mercury (II) onto Activated Carbon from Rosmarinus officinalis Leaves. American Journal of Analytical Chemistry. 2015;06(01):1-10.
79. Tan KL, Hameed BH. Insight into the adsorption kinetics models for the removal of contaminants from aqueous solutions. Journal of the Taiwan Institute of Chemical Engineers. 2017;74:25-48.